Prediction of river temperature surges is dependent on precipitation method

Croghan, Danny; Van Loon, Anne F.; Sadler, Jon P.; Bradley, Chris; Hannah, David M.

DOI:
10.1002/hyp.13317

Document Version
Publisher's PDF, also known as Version of record

Citation for published version (Harvard):
Croghan, D, Van Loon, AF, Sadler, JP, Bradley, C & Hannah, DM 2019, 'Prediction of river temperature surges is dependent on precipitation method', *Hydrological Processes*, vol. 33, no. 1, pp. 144-159. https://doi.org/10.1002/hyp.13317

Received: 22 June 2018 | Accepted: 25 October 2018

DOI: 10.1002/hyp.13317

RESEARCH ARTICLE

WILEY

Prediction of river temperature surges is dependent on precipitation method

Danny Croghan | Anne F. Van Loon | Jon P. Sadler | Chris Bradley | David M. Hannah

School of Geography, Earth and Environmental Sciences, University of Birmingham, Birmingham, UK

Correspondence
Danny Croghan, School of Geography, Earth and Environmental Sciences, University of Birmingham, Birmingham B15 2TT, UK.
Email: dxc959@bham.ac.uk

Funding information
Engineering and Physical Sciences Research Council studentship, Grant/Award Number: 1673769

Abstract

Urban river systems are particularly sensitive to precipitation-driven water temperature surges and fluctuations. These result from rapid heat transfer from low-specific heat capacity surfaces to precipitation, which can cause thermally polluted surface run-off to enter urban streams. This can lead to additional ecological stress on these already precarious ecosystems. Although precipitation is a first-order driver of hydrological response, water temperature studies rarely characterize rain event dynamics and typically rely on single gauge data that yield only partial estimates of catchment precipitation. This paper examines three precipitation measuring methods (a statutory automatic weather station, citizen science gauges, and radar estimates) and investigates relationships between estimated rainfall inputs and subhourly surges and diurnal fluctuations in urban river water temperature. Water temperatures were monitored at 12 sites in summer 2016 in the River Rea, in Birmingham, UK. Generalized additive models were used to model the relationship between subhourly water temperature surges and precipitation intensity and subsequently the relationship between daily precipitation totals and standardized mean water temperature. The different precipitation measurement sources give highly variable precipitation estimates that relate differently to water temperature fluctuations. The radar catchment-averaged method produced the best model fit (generalized cross-validation score [GCV] = 0.30) and was the only model to show a significant relationship between water temperature surges and precipitation intensity ($P < 0.001$, $R^2 = 0.69$). With respect to daily metrics, catchment-averaged precipitation estimates from citizen science data yielded the best model fit (GCV score = 0.20). All precipitation measurement and calculation methods successfully modelled the relationship between standardized mean water temperature and daily precipitation ($P < 0.001$). This research highlights the potential for the use of alternative precipitation datasets to enhance understanding of event-based variability in water quality studies. We conclude by recommending the use of spatially distributed precipitation data operating at high spatial (<1 km^2) and temporal (<15 min) resolutions to improve the analysis of event-based water temperature and water quality studies.

KEYWORDS

citizen science, event analysis, precipitation, radar, urban hydrology, water quality, water temperature

1 | INTRODUCTION

Urban stream water temperatures are highly variable and subject to short-term changes during high-intensity precipitation events. Although of short duration, event-based changes, hereafter referred to as water temperature "surges," can affect urban stream ecosystem health (Anderson, Anderson, Thaxton, & Babyak, 2010; Herb, Janke, Mohseni, & Stefan, 2008; Hester & Bauman, 2013; Hofmeister, Cianfrani, & Hession, 2015; Jones, Hunt, & Winston, 2012; Nelson & Palmer, 2007; Pluhowski & Pecora, 1970; Somers et al., 2013; Somers, Bernhardt, McGlynn, & Urban, 2016; Thompson, Kim, & Vandermuss, 2008). Water temperature is a controlling factor on a wide range of abiotic and biotic variables. Hence, sudden changes can have a cascade effect on a multitude of temperature-driven processes (Webb, Hannah, Moore, Brown, & Nobilis, 2008) particularly in urban catchments where regular surge effects can contribute to the "urban stream syndrome" (Walsh et al., 2005). Although water temperature surges occur over very short time scales (minutes to hours), precipitation also influences water temperature regimes over longer temporal scales (Hannah & Garner, 2015). The influence of precipitation on diurnal urban water temperature dynamics has not been studied extensively. Precipitation can decouple diurnal temperature from air temperature influence, leading to a distinct diurnal response in water temperature dynamics (Constantz, 1998). Resultantly, large precipitation events may impact river water temperatures change over longer time periods than previously thought.

Urban environments are vulnerable to water temperature surges due to rapid heat-transfer between precipitation and surfaces with a low specific heat-capacity, coupled with changes in surface run-off processes in urban areas (Fletcher, Andrieu, & Hamel, 2013; Herb et al., 2008; Nelson & Palmer, 2007; Van Buren, Watt, Marsalek, & Anderson, 2000). Urban surfaces are typically darker in colour and have a low specific heat-capacity; they can heat quickly and reach temperatures that far exceed air temperature on warm days. During precipitation events, heat can be rapidly transferred from these surfaces to surface run-off. As this thermally polluted run-off enters rivers, rapid increases in river water temperature can occur (Herb et al., 2008; Van Buren et al., 2000). Moreover, the high proportion of low-permeability surfaces in urban areas reduces infiltration and increases the proportion of precipitation that is conveyed rapidly through the catchment via direct surface run-off and through storm drains (Fletcher et al., 2013; Walsh, Fletcher, & Burns, 2012). Hence, a high proportion of urban precipitation is routed rapidly into water courses, with the consequence that thermally polluted run-off enters rivers in greater quantities than in natural catchments. Furthermore, due to reduced infiltration and changes in subsurface flow pathways, urban streams typically experience reductions in baseflow (Fletcher et al., 2013). This can further increase the vulnerability of urban rivers to precipitation-driven water temperature changes, thereby increasing the influence of run-off temperatures on the temperature of receiving streams.

Characterization of urban precipitation patterns requires high spatial and temporal resolution precipitation data (Berne, Delrieu, Creutin, & Obled, 2004). However, many studies lack high-density precipitation gauges to quantify urban precipitation accurately (Pedersen, Jensen, Christensen, & Madsen, 2010; Thorndahl et al., 2017). Consequently, it may be difficult to infer links between precipitation and hydrological processes in urban catchments (Berne et al., 2004). This has implications for a multitude of water quality variables that are influenced by event rainfall (Sandoval, Torres, Duarte, & Velasco, 2014; Tilburg, Jordan, Carlson, Zeeman, & Yund, 2015).

The analyses of precipitation metrics and water temperature frequently rely on single rainfall gauge data. These are often assumed to be representative of catchments with multiple water temperature logger sites (Brown & Hannah, 2007; Hester & Bauman, 2013; Hofmeister et al., 2015; Lange & Haensler, 2012; Somers et al., 2013; Somers et al., 2016; Wilby, Johnson, & Toone, 2015). However, precipitation typically exhibits high spatial variability within catchments at different scales (Dixon & Mote, 2003; Salvadore, Bronders, & Batelaan, 2015). This is particularly evident in urban catchments where the combination of the urban heat island effect and changes in urban wind field alter precipitation patterns (Dixon & Mote, 2003; Salvadore et al., 2015) leads to variations in rainfall intensity and duration (Gabriele, Chiaravalloti, & Procopio, 2017; Pedersen et al., 2010; Thorndahl et al., 2017; Villarini, Mandapaka, Krajewski, & Moore, 2008). Consequently, the precipitation processes that drive water temperature fluxes during individual events can be difficult to quantify, particularly when using data from a single rainfall gauge.

Radar and citizen science precipitation datasets may provide a useful alternative to single rainfall gauges (Buytaert et al., 2014; Gabriele et al., 2017; Koch & Stisen, 2017; Starkey et al., 2017; Thorndahl et al., 2017), particularly in urban catchments where high-spatial resolution precipitation data are required or where catchments are poorly gauged (Berne et al., 2004). Citizen science precipitation databases are increasingly common and can potentially increase the number of precipitation gauges available for catchment studies (Koch & Stisen, 2017; Starkey et al., 2017). However, to-date concerns over data quality have inhibited their uptake for research purposes (Barthel, Seidl, Nickel, & Büttner, 2016; Buytaert et al., 2014; Starkey et al., 2017). Radar precipitation data can also yield high temporal and spatial resolution precipitation estimates (Biggs & Atkinson, 2011; Gabriele et al., 2017; Thorndahl et al., 2017; Villarini et al., 2008). For example, in the United Kingdom, the NIMROD system generates radar-derived precipitation estimates at 5-min temporal and 1-km^2 spatial resolution (Villarini et al., 2008). These systems can monitor moderate- to high-intensity precipitation events well, but they are less accurate in low-intensity precipitation events (Biggs & Atkinson, 2011; Golding, 2000). Previously, 5-min temporal resolution radar precipitation has been found to represent spatial variability of rainfall well in small, urban catchments, compared with high-density gauge networks (Berne et al., 2004; Thorndahl et al., 2017). Although radar estimates of total precipitation can be variable, the use of radar at a minimum of 5-min temporal resolution can provide good precipitation estimates for urban hydrology applications (Einfalt et al., 2004; Rico-Ramirez, Liguori, & Schellart, 2015).

This paper investigates the use of different precipitation data sources in urban river water temperature studies, motivated by improving our understanding of water temperature fluxes during rainfall events. We aim to establish which type of precipitation estimate correlates strongest with subhourly and daily water temperature change with the following objectives:

1. Quantify how precipitation captured by citizen science and radar precipitation datasets compare with automatic weather stations providing point-based source estimates in the prediction of river-water temperature fluctuations over subhourly and daily timescales.
2. Explore to what extent three precipitation datasets are able to represent spatial variability in precipitation intensity in relation to a water temperature surge event

2 | METHODS

2.1 | Study location

The study was undertaken in the catchment of the River Rea in Birmingham, West Midlands, UK (52.4862° N, 1.8904° W; Figure 1 a). This headwater catchment is located within the second largest urban conurbation within the United Kingdom (Figure 1b). The 74-km^2 catchment comprises clay overlying sandstone, with 31% of the catchment defined as highly permeable bedrock, particularly in the centre of the catchment (NRFA, 2018). Surface elevations range from 107 to 291 m asl and mean annual precipitation of 781 mm (NRFA, 2018). Precipitation in the catchment exhibits a seasonal pattern, with the highest precipitation generally occurring from October to December, with the driest months from February to May (NRFA, 2018). The dominant Lamb weather type within the catchment is anti-cyclonic, with this the dominant weather type throughout the year, although cyclonic conditions occur with increased frequency during the summer months (Zhang, Cai, & Thornes, 2014). The proportion of the catchment that is urbanized is extremely high (built-up urban: 70.2%) making it an ideal study catchment for the effects of urbanization: The remaining land use mainly comprises urban green space. The high proportion of storm drains and low-permeability surfaces in the catchment leads to a dominance of rapid flow pathways that route surface run-off quickly to the river during storm events. The presence of widespread low specific heat-capacity surfaces also leads to warming of land surfaces within the summer months, priming the catchment for water temperature surge events. As a result of its land use, the Rea has a flashy flow regime with a mean flow of 0.77 m^3/s and peak flow of 73.8 m^3/s during the study period for a gauge located at the catchment outlet (NRFA, 2018).

2.2 | Data collection

2.2.1 | Water temperature data collection

River water temperatures were monitored using 12 TinyTag aquatic temperature loggers (Gemini Data Loggers, 2017) installed and calibrated using the protocol of Hannah, Malcolm, and Bradley (2009). The TinyTag loggers have a measurement accuracy of ±0.2°C and were calibrated using an ice bath set at a starting temperature of 0°C in which they were placed for 48 hr with temperature logged at 15-min intervals recording in British Summer Time and starting on the hour, in accordance with the precipitation datasets. The mean water temperature logged in the ice bath was then determined, and correction factors were calculated for individual TinyTags which either

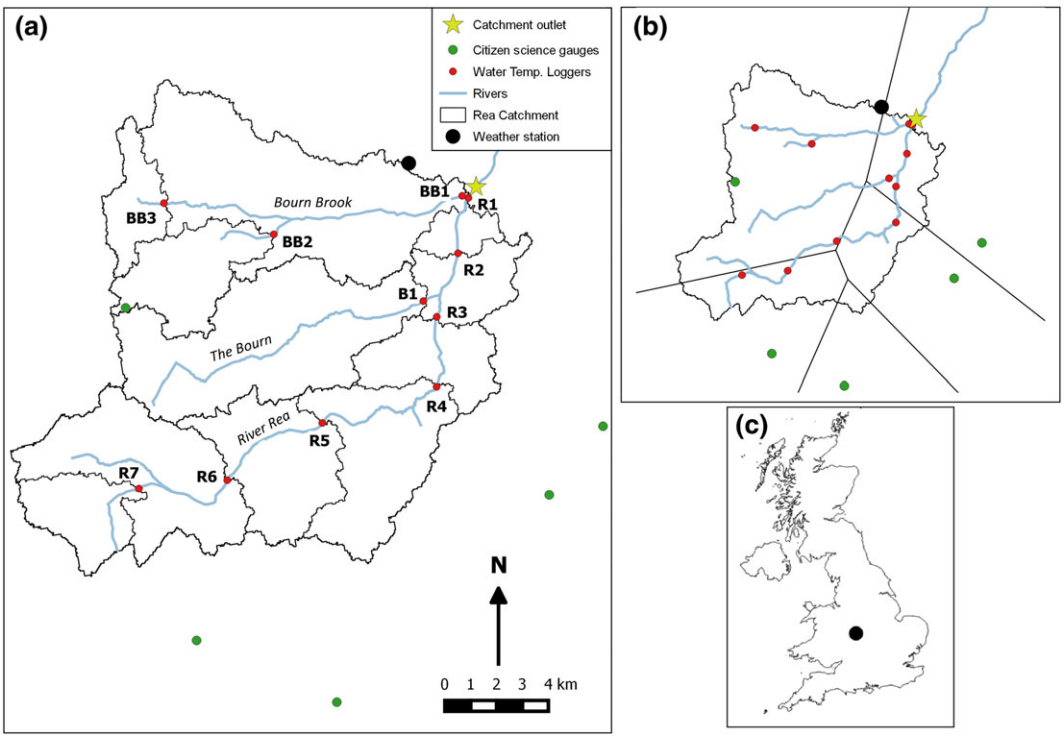

FIGURE 1 The River Rea catchment, UK. (a) Locations of water temperature loggers, automatic weather station, and citizen science gauges, and site names; (b) The contributing area of each citizen science gauge to the Thiessen polygon; (c) The location of the Rea catchment within the United Kingdom

underestimated or overestimated water temperatures compared with the mean. Correction factors were applied postmonitoring.

To monitor the water column temperature, TinyTags were secured to the riverbed in areas of unimpeded perennial flow. The loggers were placed within white radiation shields to prevent atmospheric radiation directly warming the loggers and placed parallel to the flow to ensure constant flow through the radiation shield (Hannah et al., 2009). Loggers were tied to iron bars buried into the stream bed with wire rope and left free floating in the middle of the river stream, to prevent debris build-up impeding flow to the logger. The length of the wire rope was adjusted to ensure loggers would not be washed out. Loggers were placed evenly throughout the catchment and at tributary confluences to ensure a high spatial resolution for water temperature monitoring in the catchment. This enabled localized water temperature fluxes to be monitored in line with previous studies of event-based water temperature changes (Hofmeister et al., 2015; Somers et al., 2013, 2016; Wilby et al., 2015). Loggers were installed with a mean distance between loggers of 2.5 km. Placement of loggers in some areas was impeded by lack of access to the river and hence a uniform separation distance between loggers was not feasible. For example, the Bourn tributary (Figure 1) contained only one logger (located at the tributary mouth) as the stream is largely culverted and inaccessible. The loggers were operational during the summer of 2016 (June 1, 2016, to September 15, 2016), with river-water temperatures logged at 15-min intervals. Loggers were checked once during the study period to ensure no debris build-up had occurred around the loggers which might have potentially affected the temperature data; however, no debris build-up occurred during the study period. One logger was lost during the study period, leaving data from 11 loggers available for subsequent analysis (Figure 1).

2.2.2 | Precipitation data collection

Precipitation data were collected from three available sources. First, data were obtained from a weather station (elevation 140 m asl) located near the catchment outlet which was installed prior to the study. This is a Met Office (the U.K.'s national weather service) approved station operating at 1-min temporal resolution and providing a dataset which is representative of the precipitation data used in many water temperature studies (Brown & Hannah, 2007; Hofmeister et al., 2015; Somers et al., 2016). Data were recorded in Greenwich Mean Time (GMT) and converted to British Summer Time to match the TinyTag water temperature data logging times. Distances from the weather station to individual water temperature sites ranged from 1 to 8.5 km. The use of more weather stations would have been desirable; however, further Met Office sites were too far away from the study catchment, and the creation of a dense network of gauges would have been expensive and difficult to maintain, as is the case for many water temperature studies which are reliant on single gauges (Brown & Hannah, 2007; Hester & Bauman, 2013; Hofmeister et al., 2015; Lange & Haensler, 2012; Somers et al., 2013, 2016; Wilby et al., 2015). Air temperature data used within the study were also gathered from the Met Office site within the catchment.

Second, citizen science precipitation data were collected from the Met Office Weather Observation Website (WOW; Met Office, 2018). The WOW network allows participants to upload data automatically from personal weather stations which can be downloaded freely. Each station in the network contains metadata detailing the degree of exposure, rain gauge type, recording hours, and urban climate-zone of the station. For this study, we used stations with standard precipitation gauges, with records over >95% of the study period, the minimum threshold for inclusion in the study, and at a sampling frequency of $\leq$15 min. All sites recorded in GMT and were converted to British Summer Time. All stations recorded at time intervals beginning on the hour. This provided a pool of five citizen science gauges (ranging from 2.3–4.2 km from water temperature sites), of which four gauges were located outside the study catchment (Figure 1). Rainfall gauges outside a catchment have been successfully used for discharge estimation in ungauged catchments (Samuel, Coulibaly, & Metcalfe, 2011); hence, the citizen science gauges were considered suitable for use herein. Of the five gauges, one was located in the west of the catchment, two to the south, and two to the east. Elevation at the gauges ranged from 110 to 200 m asl, with a mean of 154 m asl. As seven of the water temperature loggers are located to the east of the catchment, the gauges to the east of the catchment have a larger weighting on precipitation estimates for these loggers. Although denser networks of citizen science gauges are possible, quality control (e.g., placement of gauges) remains problematic. It should be recognized, also, that the WOW database is relatively new and is not yet comprehensive. As citizen science gauges are reliant on maintenance and installation by amateurs, data quality is reduced compared with official sources (Buytaert et al., 2014).

Third, high resolution precipitation data from the U.K.'s NIMROD radar system were provided by the U.K. Centre for Environmental Data (Met Office, 2003). Radar data were provided at 5-min temporal and 1-km^2 spatial resolution. Data are recorded from the start of the hour onwards and converted from GMT to British Summer Time. Radar data from the NIMROD system have been quality checked and corrected through national scale corrections using gauge data, as described by Harrison, Scovell, and Kitchen (2009). Quantifying uncertainty ranges in radar rainfall has proven difficult as uncertainty propagates from a wide range of sources including, but not limited to, topography, atmospheric conditions, and distance from radar source. An extensive list of uncertainties and errors associated with radar data has been compiled by Villarini and Krajewski (2010). As the study catchment is in a relatively flat area and is situated within 50 km of the nearest radar site (the Cleft Hill radar), these uncertainties are reduced for this study.

Point-based and catchment-average estimates were derived for the three precipitation datasets. Point-based data for each water temperature logger site were taken from the nearest weather station (only one weather station was used in this study, resulting in the same data used for each logger site), citizen science gauge, or radar grid cell (at 1-km^2 resolution). For catchment-average data, nested catchments for each water temperature logger site were identified from the catchment topography, and precipitation data were averaged over each logger catchment to yield an overall catchment-average precipitation estimate. Consequently, the catchment data are less variable than point-based data, particularly for the nested catchments. Citizen science gauge precipitation was averaged using the Thiessen method

TABLE 1 List of water temperature surges in the study period

Date	Site	Water Temperature Surge	Storm Type	Weather Station Intensity	Radar Point Intensity	Radar Catchment Intensity	Citizen Point Intensity	Citizen Catchment Intensity
07/06/2016	R2	1.2	A	2.4	9.5	5.2	0	0.2
08/06/2016	R5	2.1	A	0	73.1	34.9	14.2	19
08/06/2016	R6	4.2	A	0	69.4	34.3	31.5	21.1
08/06/2016	BB3	3.8	A	96	107	46.7	31.5	31.5
08/06/2016	R4	4.2	A	96	6.4	33.8	31.5	19
08/06/2016	R7	4.9	A	84	40	36.4	9.1	17.7
08/06/2016	R1	1.1	A	14.4	70.5	20.6	7.1	24.5
08/06/2016	BB1	2.2	A	14.4	50	30.8	3.1	31.5
08/06/2016	B1	1.3	A	14.4	25.8	28.2	7.1	30.1
08/06/2016	R3	3.2	A	9.2	25.8	29.6	5.1	18.6
08/06/2016	R2	2	A	4.8	43.4	22.4	0	21.8
11/06/2016	R7	1.1	A	0	0.8	4.6	0	0
11/06/2016	R4	1.4	A	0	3.6	9.1	22.4	6.4
12/06/2016	R7	1.1	C	4.8	2	1.6	2	2.9
12/06/2016	R5	1.3	C	6.4	32.6	13.6	0	10.2
12/06/2016	R3	1.1	C	12.8	12.3	8.9	0	8.6
13/06/2016	R7	1.2	C	16	23.2	13.7	4	4.5
14/06/2016	R3	1.1	C	24	10.7	4.7	1	2.9
14/06/2016	BB2	1.4	C	0	11.9	6.4	5.1	5.1
14/06/2016	BB3	1.3	C	4.8	6.7	6.7	0	5.1
25/06/2016	R4	1.3	A	0	51.8	17.5	0	0
01/07/2016	BB2	1.1	C	0	1.5	20.6	0	9.1
12/07/2016	BB2	1.5	A	0	1.4	0.7	2	5.1
12/07/2016	R3	2.3	A	0	1.6	0.8	0	1.
28/07/2016	R7	1.8	C	4.8	3	2.9	4.1	2.7
28/07/2016	BB2	1.3	C	6	2.4	1.5	1	4.1
28/07/2016	BB2	1.4	C	2.4	25.3	12	0	0
29/07/2016	R6	1.5	C	0	7.1	4.5	1	2.7
29/07/2016	R7	2.1	C	0	5.6	4.4	1	2.2
19/08/2016	R7	1.4	C	4.8	2.2	2.2	2	2.7
19/08/2016	BB2	1.1	C	2.4	2	2.2	2	4.1
25/08/2016	BB2	1.5	A	4.8	3.8	4.4	5.1	5.1
25/08/2016	BB2	1.3	A	2.4	9.8	9.2	2	5.1
25/08/2016	BB2	1	A	19.2	9.8	9.2	3.1	5.1
27/08/2016	BB3	2.9	A	0	20	17.6	0	4.1
28/08/2016	R7	1.6	C	0	15.8	7.9	0	0
28/08/2016	R5	1	C	0	21.8	12.4	0	0
03/09/2016	BB2	1.6	A	36	11.1	9.8	18.6	18.6
03/09/2016	BB3	1.9	A	36	8.6	10.6	18.6	18.6
10/09/2016	R3	1.3	A	28.8	6.4	13.3	16.4	15.2
13/09/2016	R7	2.2	C	0	21.6	12.8	0	0.4
13/09/2016	BB2	2.8	C	6.4	7.2	21.2	8.1	8.2
13/09/2016	BB3	1.7	C	6.4	16.5	15.6	8.1	8.2
13/09/2016	R2	1.1	C	25.6	11.2	18.8	18.6	11.4
13/09/2016	B1	1.1	C	25.6	8.8	9.1	5	18.6
13/09/2016	R6	1.7	C	19.2	14.2	8.6	9	15.5
13/09/2016	BB1	1.1	C	19.2	13.3	11.3	16.3	4.9
13/09/2016	R1	1.1	C	19.2	13.3	11	16.3	9.4

Note. Site shows the location of the TinyTag logger (Figure 1), Water temperature surge shows the maximum water temperature surge extent for each event, event type refers to A (A), or Cyclonic (C). Intensity refers to maximum precipitation intensity for each surge as recorded by the different precipitation datasets.

(Figure 1c), given its simplicity and widespread use in estimating areal precipitation (Ball & Luk, 1998). The contributing area of each gauge was determined, and the contributing percentage of each gauge to each nested catchment precipitation total was calculated to derive estimates for catchment precipitation for each site. Because the weather station data featured only a single gauge, catchment-average precipitation could not be derived for this dataset. For the radar data, the contribution of each grid cell to each subcatchment were calculated, and catchment-average precipitation was then derived for each logger.

2.3 | Statistical analysis

Statistical analysis was undertaken using each of the precipitation datasets to, first, relate subhourly water temperature changes to precipitation intensity and, second, daily water temperature changes to daily precipitation.

2.3.1 | Subhourly analysis

For subhourly water temperature changes, the relationship between precipitation and water temperature surges was analysed. Here, water temperature surges were defined as positive change of at least 1°C in water temperature that occurred after the onset of a precipitation event. The threshold of a 1°C change within a 30 min time-window, measured from the onset of water temperature rise, was used to identify surges, as has been used in previous studies (Somers et al., 2016). This threshold ensured water temperature changes were caused by the precipitation event and not by air temperature influence. Forty-eight temperature surges were identified within the study period (Table 1).

Precipitation metrics linked to water temperature surges (Herb et al., 2008; Nelson & Palmer, 2007; Somers et al., 2013) were calculated for each precipitation calculation method: maximum precipitation intensity prior to the surge, precipitation in the 30 min before the surge, and the precipitation total for the event prior to the surge. Exploratory analysis revealed that results for each metric were similar; hence, only results for maximum precipitation intensity are presented herein. Precipitation intensity was selected given the importance of intense events rather than overall rainfall amount in causing water temperature surges identified in previous studies (Nelson & Palmer, 2007).

Initial analyses showed the relationship between water temperature surge and precipitation intensity to be non-linear, so general additive models (GAMs) were chosen for the analysis. GAMs are a class of generalized linear models and are ideal for semi-parametric datasets given there is no assumption of linearity and are flexible in dealing with differing (non-normal) statistical distributions of the data (Murase, Nagashima, Yonezaki, Matsukura, & Kitakado, 2009). Due to this, GAMs have been particularly useful in modelling environmental effects on water temperature (Laanaya, St-Hilaire, & Gloaguen, 2017). All models were created using the "mgcv" package in R (Wood, 2018): The equation for GAMs can be written as follows:

$$g(E(y)) = \beta\_0 + f1(x1) + f2(x2) + \ldots f_p(X_p) + \varepsilon$$

Where g is a link function, $E(y)$ is the response variables expected value, fi (xi) is the smoothed function, and ε is the error. The link function is a parametric function that enables the Gaussian error structure to be applied to an exponential family, thereby linking the average of the dependent variables to the predictor variables (Laanaya et al., 2017). The smoothed function defines the regularity of the application of the regression within the model. This is controlled by the basis dimension (k) that represents the dimensionality of the spline basis and controls the maximum degrees of freedom that can be applied within the model by each term. Higher values of k mean the smoothing function is applied more regularly.

For this study, a two explanatory variable GAM using a Gaussian error structure and identity link function was produced for all precipitation datasets. All water temperature surges in the study period were used for the model (Table 1). The difference between water temperature and air temperature was used as an additional variable alongside maximum precipitation intensity, as preliminary analysis for this study had reflected its importance. This was done to achieve better model fits and to assess how the relative importance of maximum precipitation intensity to the GAM alters depending on the precipitation dataset used. The difference between water temperature and dew point temperature was also calculated; however, this was highly

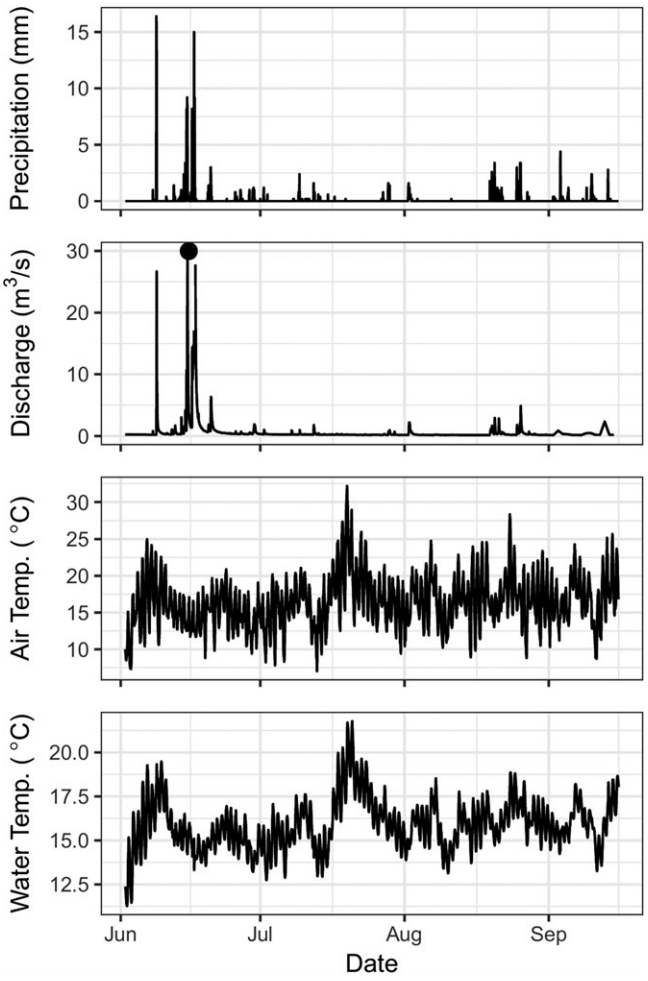

FIGURE 2 Time series for site R1 (see Figure 1) showing water temperature, air temperature, and precipitation as recorded at the weather station, and discharge as recorded as recorded at the catchment outlet. The black dot on the discharge graph shows a particularly large event that peaked at 62 m^3/s, outside the limits of the y-axis

correlated with water temperature and air temperature difference so did not feature in the final model. A smoother term was applied to the maximum precipitation intensity variable in all models, and the basis dimension (*k* value) was chosen based on generalized cross-validation (GCV; Wood, 2017). To assess the best model fit for the GAM's, GCV scores were used. GCV scores show the minimized GCV score for each GAM, with a lower score indicating a better fitting model with less predictive error.

For an example storm on June 8, 2016, maximum water temperature surges for each logger site were regressed against maximum precipitation intensity, with models produced for each type of precipitation dataset in the study. The adjusted r^2 was then compared to assess which precipitation dataset had the highest explanatory capability. The event in June 8 was chosen as it had the largest water temperature surges in the study period, whereas the event on September 13, 2016, did not feature a regression due to low sample size. A lower

TABLE 2 Precipitation (mm) for summer months in 2016 at the weather station site

	June	Difference (%)	July	Difference (%)	August	Difference (%)	Total	Difference (%)
Radar average	166	−6.6	17	−23.5	47	−9.1	230	−9.1
Radar point	194	+8.8	20	−5	39	+0.8	253	+0.8
Citizen average	120	−47.5	23	+8.7	52	−28.7	195	−28.7
Citizen point	128	−38.2	26	+19.2	58	−18.3	212	−18.3
Weather station	177	NA	21	NA	53	NA	251	NA

Note. Percentage difference was calculated as percentage difference in precipitation relative to weather station site. Citizen: citizen science data; catchment: catchment-average; point: point-based.

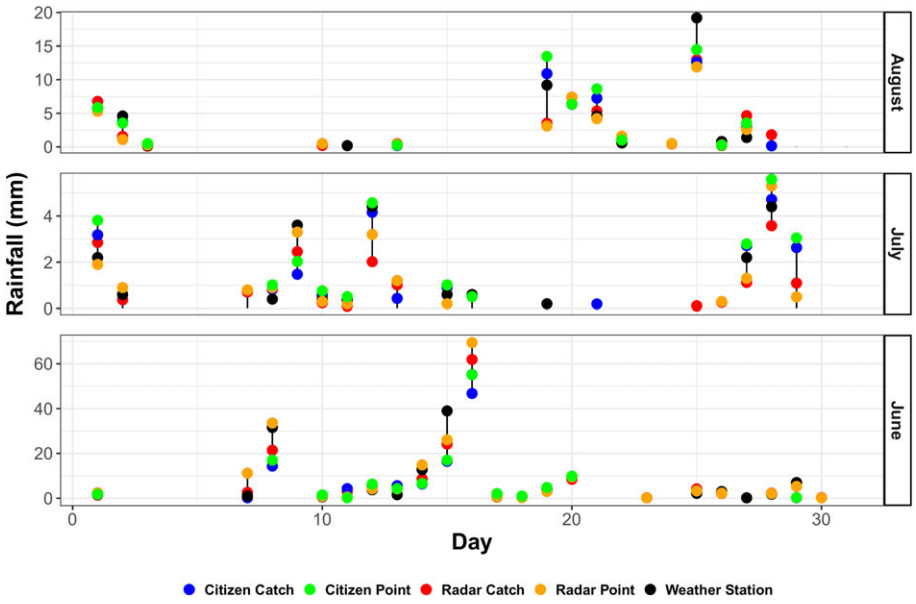

FIGURE 3 Daily precipitation totals for the study catchment. Black bars represent the daily precipitation range. Coloured dots represent the different precipitation methods used in the study

TABLE 3 Validated GAM's for maximum precipitation intensity calculated by different precipitation sources against water temperature surges

	Radar catchment			Radar point			Citizen catchment			Citizen point			Weather station		
Adjusted R^2	0.69			0.62			0.65			0.60			0.61		
Deviance explained (%)	72.7			66.7			69.5			64.5			65.4		
GCV score	0.30			0.37			0.34			0.39			0.38		
Sample size	48			48			48			48			48		
Covariate	*df*	*k*	*P* value	*df*	*k*	*P* value	*df*	*k*	*P* value	*df*	*k*	*P* value	*df*	*k*	*P* value
Maximum precipitation intensity	1.7	3	<0.001	1.7	3	0.30	1.7	3	0.056	1.4	3	0.36	1.15	3	0.17
Starting water/air temperature difference	3.9	5	<0.01	3.9	5	<0.001	3.9	5	<0.001	3.9	5	<0.001	3.9	5	<0.001

Note. Citizen: citizen science data; catchment: catchment-average; point: point-based.

intensity event was also analysed for the September 13, 2016, but did not feature a regression due to low sample size.

2.3.2 | Daily analysis

For daily water temperature variability, the following temperature metrics were calculated: daily maximum, daily minimum, daily mean, and daily range. All metrics and associated precipitation data were calculated from midnight to midnight across the study period. The influence of seasonality was removed by subtracting a 10-day moving average (5 days either side) for each metric from the corresponding metric for each day. GAMs, with a Gaussian error structure and identity link function, were used to link standardized water temperature metrics to the precipitation total following the same model described in Section 2.3.1. Only precipitation days >4 mm were included in the analysis, to include only events that produced enough storm water to have a substantial effect on discharge. This threshold was derived based on a sensitivity analysis of discharge to precipitation, with 4 mm of daily precipitation being the threshold where daily discharge was consistently twice that of baseflow. As a similar relationship is shown between all calculated temperature metrics and daily precipitation, only the GAMs for the daily mean temperature metric are presented here as an example. GCV scores were again used to assess the model with the best fit.

3 | RESULTS

3.1 | Thermal, meteorological, and hydrological context

Time series for precipitation, discharge, air temperature, and water temperature are shown for the study period at site R1 (Figure 1) in

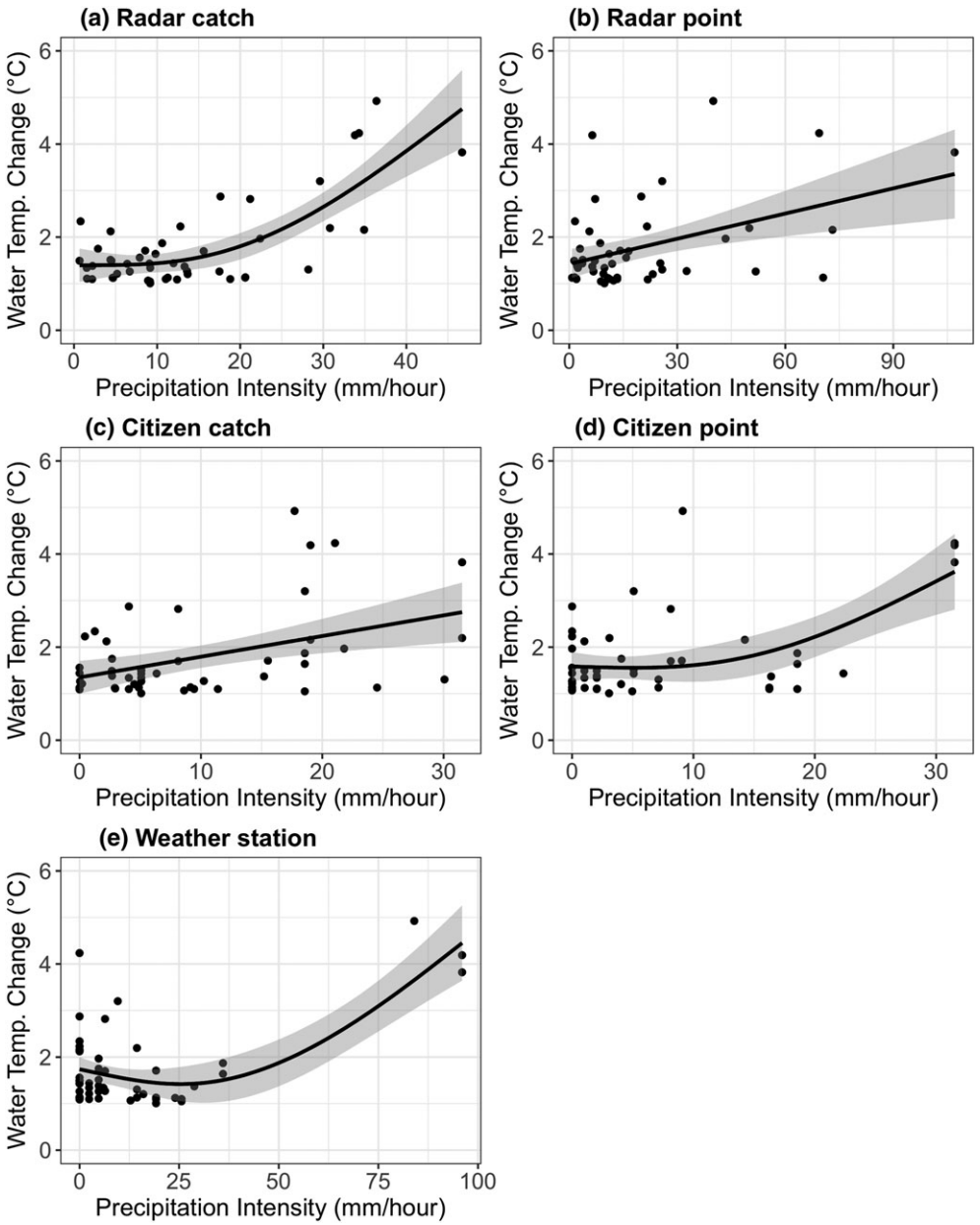

FIGURE 4 GAM's of maximum precipitation intensity and water temperature surge determined by the different precipitation sources. The black line shows the fitted line of the GAM, whereas the shaded grey area shows the 95% confidence interval

Figure 2. June was notably the wettest month in the study period, registering 174 mm of rainfall, whereas July was the driest registering 24 mm. Air temperature during the study ranged from 7°C to 32°C, with a mean of 16.3°C, whereas water temperature ranged from 11.1°C to 21.7°C, with a mean of 15.9°C. Discharge had a minimum flow of 0.14 m^3/s, with a peak flow of 61.8 m^3/s.

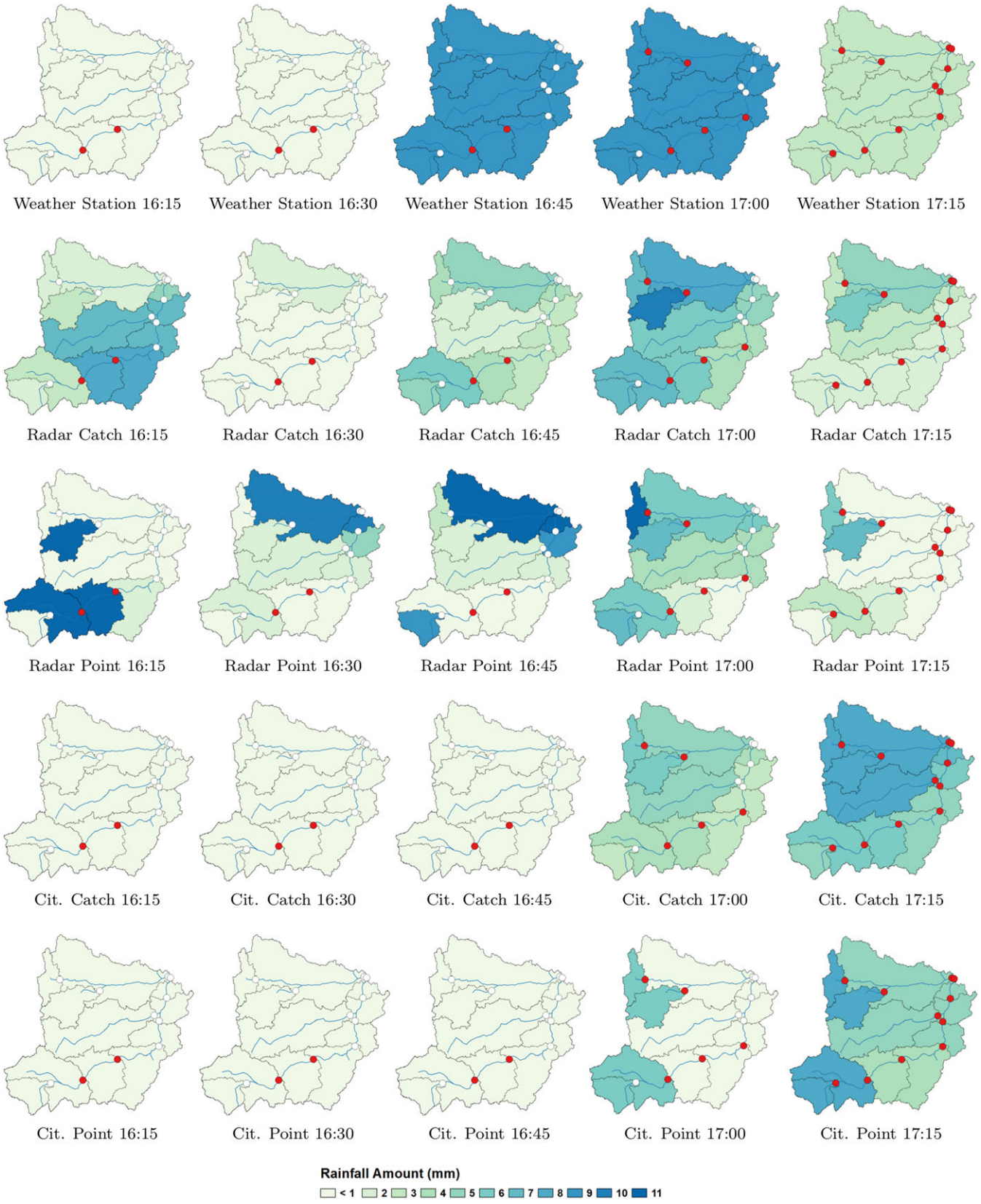

FIGURE 5 Temporal development of the event on June 8, 2016, for the different precipitation methods: White circles show no water temperature surge; red indicate >1° rise in water temperature for that site. Colours indicate precipitation in mm. Maps created in GIS by colouring in each logger nested catchment with corresponding precipitation amount for time period

3.2 | Comparison of precipitation methods

Monthly (Table 2) and daily (Figure 3) precipitation totals are shown for June, July, and August for the weather station location. The study period included months with very high (June), low (July), and mean (August) rainfall, providing a wide range of event types. Table 2 gives the percentage difference in estimated precipitation for the different precipitation methods and the weather station. In the wettest month (June), high variation was apparent. Both citizen science methods considerably underestimated precipitation in comparison to the weather station, whereas both radar methods overestimated precipitation but by a much smaller amount than citizen science methods. In the driest month (July), all methods measured relatively similar precipitation totals, although percentage differences are large given the small precipitation totals. In August, both radar methods underestimated precipitation in comparison to the weather station, particularly the radar point-based data. In August, citizen science data produced values closest to those of the weather station. The catchment citizen science data slightly underestimated compared to a slight overestimation for the citizen point-based data.

3.3 | Subhourly water temperature change

Summaries of the GAM's modelling water temperature surge using the predictors maximum precipitation intensity and air/water temperature differences are shown in Table 3. Maximum precipitation intensity was found to be a significant predictor ($P < 0.001$) of water temperature surges only when using radar catchment-average precipitation data. In contrast, maximum precipitation intensity was not found to be significant ($P > 0.05$) in any of the other GAMs. The deviance explained varied between models, ranging from 72.7% for the radar catchment-average data to 64.5% for the citizen science point-based data. Adjusted R^2 values ranged from 0.69 for the radar catchment-average GAM to 0.60 for the citizen point-based GAM. GCV score, which can be used as a means of estimating prediction error in models, was lowest for the model using radar catchment-average precipitation data (0.30) and highest for the model showing the citizen point-based precipitation data (0.39).

The GAM featuring radar catchment-average precipitation (Figure 4a) shows a non-linear threshold response, with increased water temperatures only at the higher maximum precipitation intensities. A similar non-linear trend is observed in both the weather station data (Figure 4e) and citizen point data (Figure 4d). In contrast, a linear trend is observed within the radar point (Figure 4b) and citizen catchment (Figure 4c) models.

3.3.1 | High-intensity example (June 8, 2016)

Spatial and temporal variation in precipitation for an event on June 8, 2016, and the associated water temperature surges are shown in Figure 5. Timing of precipitation differs substantially between precipitation methods. The weather station data provide only one rainfall value across the catchment with the heaviest rainfall occurring at 16:45 and 17:00. By contrast, both radar datasets show high spatial and temporal variations in rainfall across the catchment, with peak rainfall for logger sites varying between 16:15 and 16:45. The timing of peak rainfall differed markedly for logger sites between the point-based and catchment-average radar methods. Both the citizen science datasets showed minimal rainfall until 17:00, with both datasets showing peak rainfall at 17:15 for all logger sites.

The initial water temperatures surges shown at 16:15 and 16:30 appeared to occur without the onset of rainfall when using the weather station or citizen science datasets; however, both radar datasets showed rainfall correspond with these surges. Only surges occurring at 17:00 corresponded with peak rainfall at the weather station; however, substantial prior precipitation was also shown with both radar datasets. The final water temperature surges occurred by 17:15, corresponding with peak rainfall in the citizen science dataset, compared with minimal rainfall in the weather station and radar datasets.

Linear regression models show the relationship between maximum precipitation intensity and water temperature surges for the different precipitation methods in the event in June 8 (Table 4). Maximum precipitation intensity was shown to be a significant predictor only for modelled radar catchment-average data ($P < 0.001$, $R^2 = 0.54$). When using weather station, radar point-based, and citizen sciences datasets, maximum precipitation intensity was not significant with low explanatory capability shown ($P > 0.05$, $R^2 = -0.10$ to 0.14).

TABLE 4 Linear regression coefficients and adjusted R^2 for maximum precipitation intensity against water temperature surge in the event in June 8

	Estimate	Standard error	*t* value	*P* value	Adjusted R^2
Intercept	2.25	0.50	4.49	0.001	0.14
Weather station	0.15	0.01	1.63	0.138	
Intercept	−1.96	1.37	−1.43	0.185	0.54
Radar catchment	0.16	0.05	3.56	0.006	
Intercept	3.03	0.90	3.34	0.008	−0.10
Radar point	0.00	0.01	−0.26	0.796	
Intercept	5.24	1.80	2.90	0.017	0.08
Citizen catchment	−0.10	0.07	−1.37	0.202	
Intercept	2.12	0.59	3.55	0.006	0.11
Citizen point	0.04	0.02	1.49	0.169	

Note. The sample size for all models is 11.

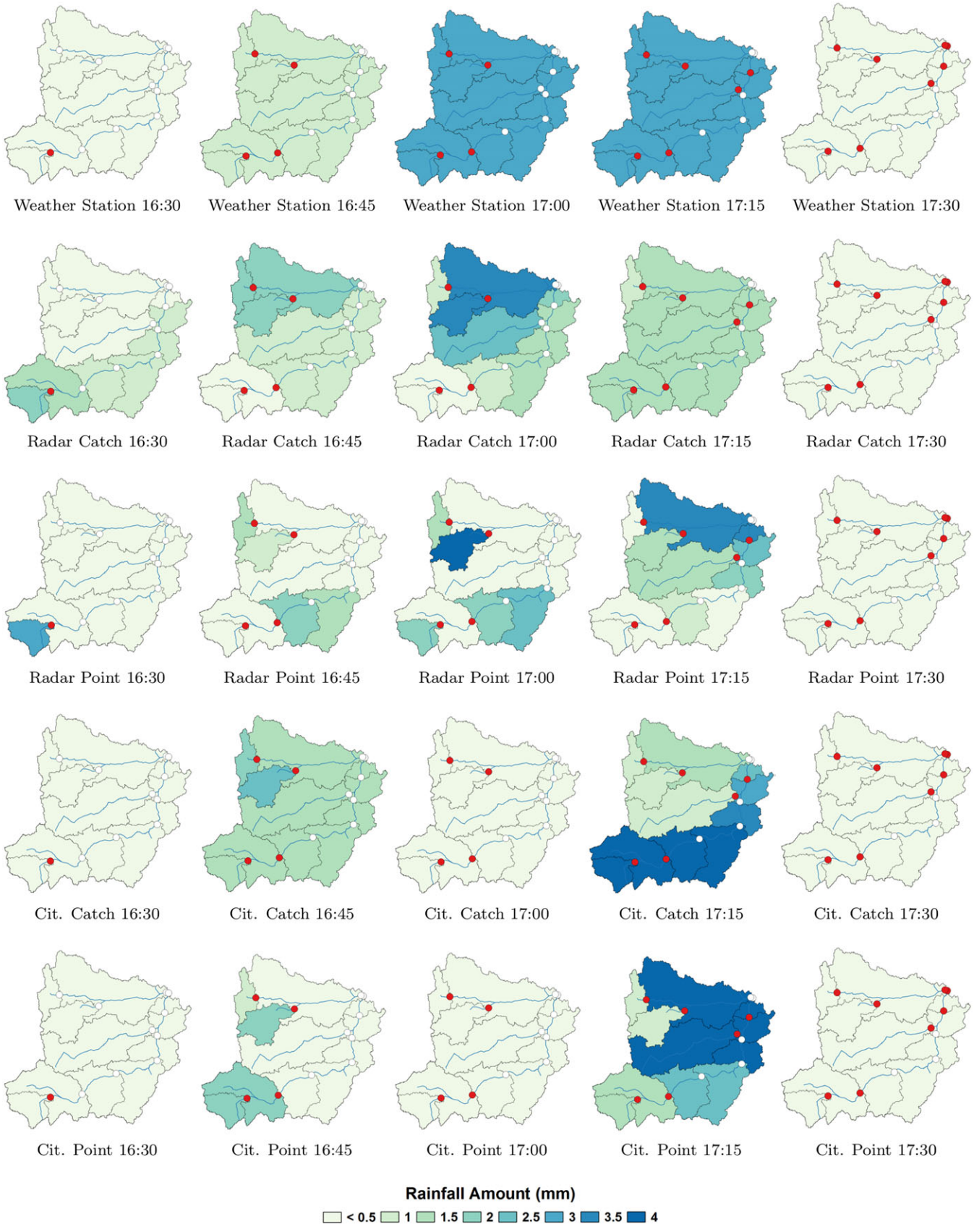

FIGURE 6 Temporal development of the event on September 13, 2016, event for the different precipitation methods: White circles show no water temperature surge; red indicate >1° rise in water temperature for that site. Colours indicate precipitation in mm. Maps created in GIS by colouring in each logger nested catchment with corresponding precipitation amount for time period

TABLE 5 Validated GAM's for standardised mean daily water temperature against daily precipitation total as determined by the different precipitation sources

	Radar catchment			Radar point			Citizen catchment			Citizen point			Weather station		
Adjusted R^2	0.18			0.20			0.41			0.41			0.50		
Deviance explained (%)	20.7			22.2			42.5			30.2			52.2		
GCV score	0.33			0.31			0.20			0.26			0.20		
Sample size	127			151			155			150			152		
Covariate	*df*	*k*	*P* value	*df*	*k*	*P* value	*df*	*k*	*P* value	*df*	*k*	*P* value	*df*	*k*	*P* value
Precipitation Total	3,2	5	<0.001	3.5	6	<0.001	4.9	6	<0.001	4.7	6	<0.001	4.9	5	<0.001

Note. Citizen: citizen science data; catchment: catchment-average; point: point-based.

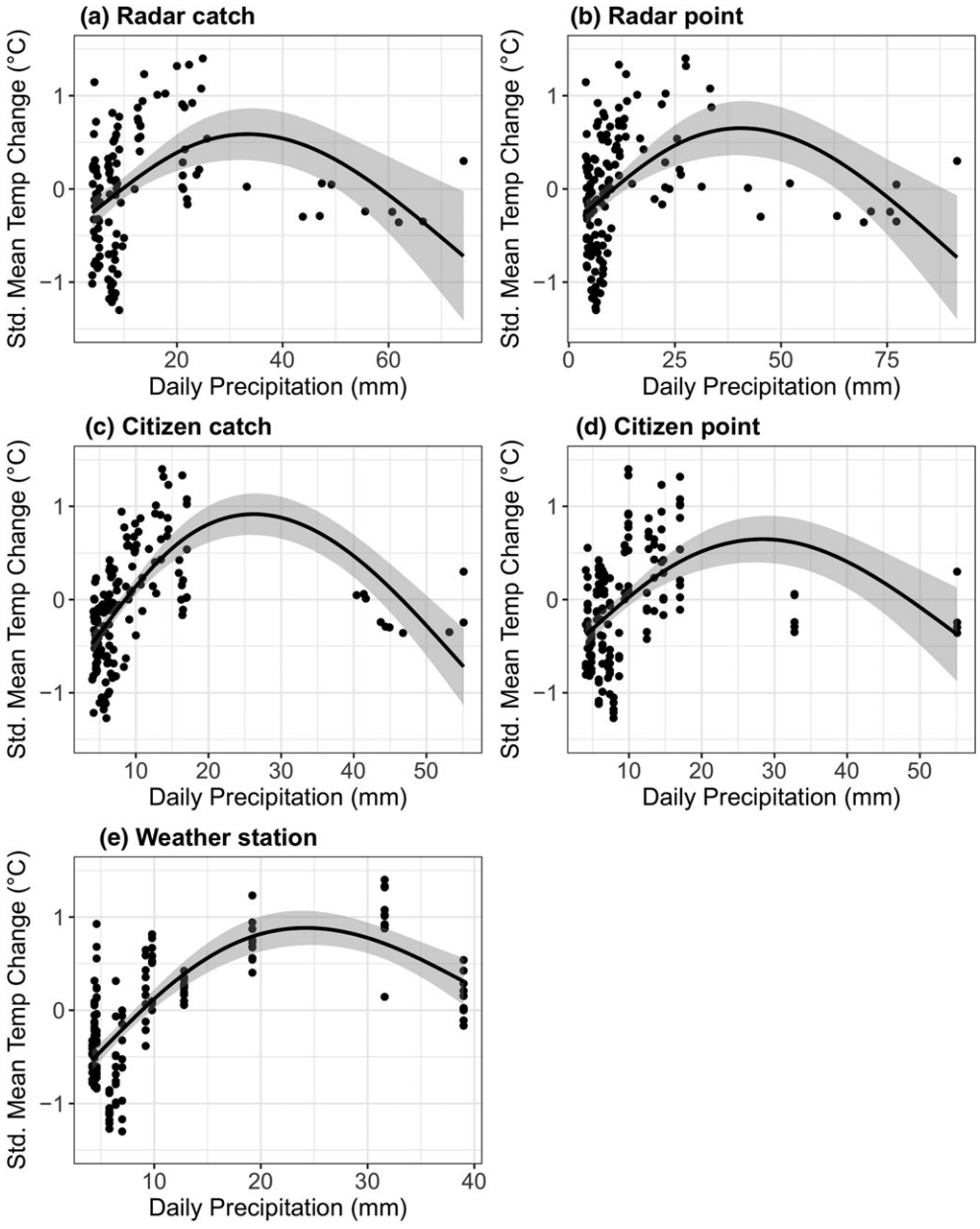

FIGURE 7 GAM's of daily precipitation and standardized mean daily water temperature determined by the different precipitation sources. All TinyTag sites are combined for the purposes of these plots. The black line shows the fitted line of the GAM, whereas the shaded grey area shows the 95% confidence interval

3.3.2 | Low-intensity example (September 13, 2016)

Spatial and temporal variations in precipitation and water temperature for a low-intensity event for September 13, 2016, are shown in Figure 6. Temporal variation through the event was lower than for the event in June 8, with all precipitation datasets suggesting that the majority of precipitation occurred between 16:45 and 17:15. Again, the weather station provided a single value across the catchment, suggesting almost all precipitation fell between 17:00 and 17:15 (after the first temperature surge event occurred). In contrast, both radar and citizen science methods indicate substantial rainfall in the south-west of the catchment prior to this, although only the radar methods capture precipitation corresponding to the initial water temperature surge at 16:30. Both citizen science and radar methods capture precipitation in the north-west of the catchment, which is the location of the subsequent water temperature surge. Large differences in precipitation estimation are noticeable at 17:00. Both citizen science methods suggest minimal precipitation at this point; however, this was the time of peak rainfall within both radar methods and at the weather station site in the north of the catchment. By contrast, peak rainfall in the citizen science sites occurred at 17:15. For the citizen science catchment method, peak rainfall is shown within the south-east of the catchment, where no surge events were identified. By contrast, both radar methods suggest minimal precipitation in this location. Two further surge events were captured at this point, with citizen point and radar point suggesting the heaviest precipitation corresponding with these. By 17:30, all methods show the event to have ended.

3.4 | Daily water temperature variability

Summaries of the GAM's modelling deviation from mean water temperature using daily precipitation amount are shown in Table 5. In all models, daily precipitation was found to be a significant predictor for standardized daily mean water temperature ($P < 0.001$). The explained deviance varied widely between models, ranging from 20.7% for the radar catchment-average GAM to 52.2% for the weather station GAM. Adjusted R^2 ranged from 0.18 for the radar catchment-average GAM to 0.50 for the weather station GAM. GCV was lowest for the citizen catchment-average precipitation model (0.20) and highest for the radar catchment-average precipitation model (0.33). A non-linear response was evident with an initial rise in standardized mean water temperature with higher precipitation totals up to a threshold around 20 mm which is followed by a fall in standardized mean water temperature for the highest daily precipitation totals was shown by all models (Figure 7).

4 | DISCUSSION AND CONCLUSIONS

4.1 | Precipitation estimate differences between datasets

Differences in precipitation between datasets (weather station, citizen science, and radar) were more pronounced than the differences between point-based and catchment-average calculation methods, which reflect precipitation variability over short distances during the events. Single precipitation gauge data are, therefore, often unrepresentative of multiple water temperature sample sites unless strict consideration is given to catchment size and strategic siting (Gabriele et al., 2017; Thorndahl et al., 2017; Villarini et al., 2008).

Citizen science estimates of precipitation were highly inaccurate with respect to percentage difference in total rainfall amount, compared with estimates at the weather station site location, during high-intensity events, possibly resulting from high spatial variability in precipitation within the catchment that was not adequately accounted for by the citizen science gauges (Pedersen et al., 2010). These errors may also propagate from siting issues as meteorological standards for gauge site siting may be difficult to adhere to for citizens in urban areas due to lack of unobstructed space, which may lead to underestimation of precipitation (Muller, Chapman, Grimmond, Young, & Cai, 2013). Radar data were most accurate in the wettest month (August) but exhibited substantial discrepancies from the weather station gauge in the driest month (June), possibly as radar data have larger uncertainty at lower precipitation intensities as radar data struggles to identify drizzle (Golding, 2000).

4.2 | Subhourly water temperature changes

The best model fit was achieved using the Radar catchment-average precipitation dataset. Catchment-average precipitation estimates account for precipitation falling across the catchment so are more spatially representative of "true" precipitation patterns input into the river system (Fletcher et al., 2013; Walsh et al., 2012). Radar data have previously also been shown to monitor high-intensity events accurately (Biggs & Atkinson, 2011). Consequently, the higher predictive capability of the radar catchment-average model compared with the citizen catchment-average model reflects the higher spatial and temporal resolution of the radar dataset (Gabriele et al., 2017). As water temperature surges are more likely to occur where there is rapid surface and shallow subsurface drainage (Nelson & Palmer, 2007; Somers et al., 2013), the radar catchment dataset is likely to be more representative of thermally polluted water in the river than alternative precipitation datasets. Furthermore, as the process of heat exchange between low-heat capacity surfaces and surface run-off occurs over short durations (Herb et al., 2008), this effect is likely to be better captured by the highest temporal resolution datasets. In contrast, point-based methods provide inaccurate precipitation estimates as they fail to account for variations in storm intensity across the catchment, which may result in high spatial variation in rainfall, particularly in urban areas (Thorndahl et al., 2017). Point-based methods are unlikely to be an adequate proxy of thermally charged surface run-off, as they fail to represent the export of heated water from individual subcatchments. Hence, point-based methods are particularly ineffective within urban environments, as they lack the spatial representativeness required to account for drainage systems that rapidly route water from the entire subcatchment to the river rapidly (Jones et al., 2012), which in turn leads to water temperature surges. This is particularly evident during convective storms which are responsible for most events causing

water temperature surges (Hofmeister et al., 2015; Nelson & Palmer, 2007; Wilby et al., 2015). Consequently, point-based methods are unlikely to be representative; therefore, catchment-average radar precipitation datasets are recommended for use in water temperature studies focusing on high-intensity events.

In the example water temperature surge events, both point-based and catchment-average radar estimation methods represented the relatively higher accuracy of radar data in spatially and temporally representing a high-intensity event. The close temporal proximity of the onset of high-intensity precipitation event to the water temperature surges within urbanized catchments as shown by the radar data has been observed in previous studies (Anderson et al., 2010; Hofmeister et al., 2015; Nelson & Palmer, 2007; Somers et al., 2013) which noted the quick onset of surges after localized precipitation, with a longer lag time downstream due to dissipation of heat pulses from upstream (Somers et al., 2013; Wilby et al., 2015). Alternatively, the transit time of water from the point in the catchment where the rain fell to the river may also explain the seemingly delayed water temperature surge at the most downstream sites. It is further important to consider that water temperature dynamics such as water temperature surges are also controlled by numerous other parameters such as dew point temperature that are not accounted for by solely using precipitation data (Herb et al., 2008). In contrast, for the low-intensity event, both radar methods provided a relatively accurate description of precipitation associated with water temperature surges, which contrasts with previous studies suggesting that radar data are less effective at lower rainfall intensities (Biggs & Atkinson, 2011; Golding, 2000). Furthermore, both point-based and catchment-based radar methods also gave similar estimates, suggesting lower spatial variability in the low-intensity event.

From the weather station data, only constant precipitation across the catchment could be derived, which misleadingly shows water temperature surges taking place before any precipitation was observed in both the high-intensity event and the low-intensity event. The assumption of a constant precipitation value across the catchment is likely to be highly inaccurate and leads to difficulties quantifying precipitation-driven processes (Thorndahl et al., 2017). The degree to which water temperature surges are controlled by precipitation may be underestimated or masked entirely when using single gauge data depending on catchment area, river network properties, storm direction, and rate of passage through the catchment.

Both citizen science point-based and catchment-average methods suggested that the precipitation peak occurred after the water temperature surge at five of the 10 logger sites within the high-intensity event. This represents the influence of gauges to the east of the catchment, with the June 8 storm moving from west to east across the catchment. As most of the water temperature loggers were located in the eastern part of the catchment, the precipitation estimate for them was derived from gauges to the east of the catchment. Because the rain reached these gauges later, water temperature surges were already present at these sites before precipitation was measured. Increased density of citizen gauges in the western part of the catchment would likely help better capture similar surge-triggering events. However, without high-density gauge networks with relatively even spacing, it appears that using citizen science gauge networks can lead to substantial underestimation or overestimation in high-intensity events making links to water temperature data problematic. However, for the low-intensity event, citizen point data corresponded well with water temperature surges at individual subcatchments and suggested similar spatial distributions in precipitation as the radar methods. The citizen science catchment method gave substantially different estimations, with high precipitation estimates in the south-east region of the catchment that did not feature any water temperature surges, and minimal precipitation was estimated by the point citizen science method and radar methods. This suggests that the density of citizen science gauges was not high enough to provide reliable interpolations for the low-intensity event.

4.3 | Daily water temperature variability

All precipitation calculation methods modelled the relationship between mean water temperature and total daily precipitation effectively. Strong fits were provided by all models. This is because daily metrics are less sensitive to issues related to storm timing and duration (Fletcher et al., 2013; Jacobson, 2011). This may be because the main process driving the change in daily temperature dynamics after precipitation is a change in the specific heat-capacity of the receiving waters (Hannah, Webb, & Nobilis, 2008). At higher discharges, the specific heat capacity of the stream is increased, and the river is more resilient to atmospheric cooling. As only a small subset of overall events lead to water temperature surges, diurnal temperature fluctuations after precipitation are likely to reflect changes in total discharge. Hence, although lower spatial and temporal resolution datasets may be inadequate for analyses of thermally polluted waters immediately entering rivers, lower spatial and temporal resolution precipitation datasets can provide a proxy of discharge. Therefore, if the focus of study is daily temperature metrics, then high spatial and temporal resolution precipitation data are not necessarily required.

Although citizen science and weather station datasets showed the strongest model fits, this may be an artefact of the reduced variation in rainfall in the point-based datasets which can lead to misleadingly small error in statistical models. Although radar catchment precipitation showed the worst model fit, the greater spatial variation in precipitation patterns accounted for than other methods in turn may lead to larger errors (Gabriele et al., 2017; Pedersen et al., 2010). As such, caution is required in interpreting the strength of relationships within water temperature models where precipitation is a predictor, particularly where only a single gauge is used. Furthermore, some degree of uncertainty in the analyses were caused by the timing of the events, and the possibility that precipitation from a single event may extend over 2 days. All logger sites were included in the analyses, meaning headwater and downstream sites were also mixed together, which therefore respond differently to precipitation properties.

4.4 | Implications and future research

This study highlights the value of using radar catchment-average rainfall datasets when modelling event-based water temperature fluxes at short temporal scales. However, when using traditional gauge

methods, linking precipitation to water temperature dynamics has much greater potential for error at subhourly scales, and the role of precipitation as an important variable driving water temperature dynamics may currently be underestimated or ignored. The errors that propagate from the use of single point-based sources are likely to also occur for other water quality parameters where precipitation is a primary driver of water quality dynamics. The use of catchment-average radar rainfall data as a means of analysing precipitation-led fluxes in water quality variables is therefore encouraged. High spatial and temporal variability precipitation sources such as catchment-average radar are likely to be particularly beneficial within urban water quality studies, where precipitation is shown to be more localized and where precipitation linkages to water quality dynamics can often be directly correlated. The alternative catchment-average based datasets are likely to also be advantageous to water quality studies within poorly gauged catchments.

Further research is required in catchments of different sizes and land use types. As the study took place in an urban headwater catchment, it would be useful to assess different precipitation datasets in varying land uses where hydrological and water temperature responses to precipitations events are likely to differ. To build on the findings of this study, more systematic examination of the lag time between precipitation and water temperature surges will further enhance understanding of the link between precipitation and water temperature change. Moreover, further water quality parameters could be analysed to ensure greater transferability of the results of this study to future water quality studies. Variables with a clear first flush effect, such as nutrients, organic matter, and heavy metals are of particular interest for further study given the links between catchment transport of these variables and precipitation intensity.

FUNDING INFORMATION

This research was supported by an Engineering and Physical Sciences Research Council studentship awarded to Danny Croghan grant 1673769.

ACKNOWLEDGMENTS

This research was supported by an Engineering and Physical Sciences Research Council studentship awarded to Danny Croghan grant 1673769. We thank Richard Johnson for providing for logistical support in installing the water temperature sensors.

ORCID

Danny Croghan http://orcid.org/0000-0003-1857-2528
David M. Hannah http://orcid.org/0000-0003-1714-1240

REFERENCES

Anderson, W. P., Anderson, J. L., Thaxton, C. S., & Babyak, C. M. (2010). Changes in stream temperatures in response to restoration of groundwater discharge and solar heating in a culverted, urban stream. *Journal of Hydrology*, *393*(3–4), 309–320. https://doi.org/10.1016/J.JHYDROL.2010.08.030

Ball, J. E., & Luk, K. C. (1998). Modeling spatial variability of rainfall over a catchment. *Journal of Hydrologic Engineering*, *3*(2), 122–130. https://doi.org/10.1061/(ASCE)1084-0699(1998)3:2(122)

Barthel, R., Seidl, R., Nickel, D., & Büttner, H. (2016). Global change impacts on the Upper Danube Catchment (Central Europe): A study of participatory modeling. *Regional Environmental Change*, *16*(6), 1595–1611. https://doi.org/10.1007/s10113-015-0895-x

Berne, A., Delrieu, G., Creutin, J.-D., & Obled, C. (2004). Temporal and spatial resolution of rainfall measurements required for urban hydrology. *Journal of Hydrology*, *299*(3–4), 166–179. https://doi.org/10.1016/J.JHYDROL.2004.08.002

Biggs, E. M., & Atkinson, P. M. (2011). A comparison of gauge and radar precipitation data for simulating an extreme hydrological event in the Severn Uplands, UK. *Hydrological Processes*, *25*(5), 795–810. https://doi.org/10.1002/hyp.7869

Brown, L. E., & Hannah, D. M. (2007). Alpine stream temperature response to storm events. *Journal of Hydrometeorology*, *8*(4), 952–967. https://doi.org/10.1175/JHM597.1

Buytaert, W., Zulkafli, Z., Grainger, S., Acosta, L., Alemie, T. C., Bastiaensen, J., … Zhumanova, M. (2014). Citizen science in hydrology and water resources: Opportunities for knowledge generation, ecosystem service management, and sustainable development. *Frontiers in Earth Science*, *2*, 26. https://doi.org/10.3389/feart.2014.00026

Constantz, J. (1998). Interaction between stream temperature, streamflow, and groundwater exchanges in alpine streams. *Water Resources Research*, *34*. https://doi.org/10.1029/98WR00998

Dixon, P. G., & Mote, T. L. (2003). Patterns and causes of Atlanta's urban heat island–Initiated precipitation. *Journal of Applied Meteorology*, *42*(9), 1273–1284. https://doi.org/10.1175/1520-0450(2003)042<1273:PACOAU>2.0.CO;2

Einfalt, T., Arnbjerg-Nielsen, K., Golz, C., Jensen, N.-E., Quirmbach, M., Vaes, G., & Vieux, B. (2004). Towards a roadmap for use of radar rainfall data in urban drainage. *Journal of Hydrology*, *299*(3–4), 186–202. https://doi.org/10.1016/J.JHYDROL.2004.08.004

Fletcher, T. D., Andrieu, H., & Hamel, P. (2013). Understanding, management and modelling of urban hydrology and its consequences for receiving waters: A state of the art. *Advances in Water Resources*, *51*, 261–279. https://doi.org/10.1016/j.advwatres.2012.09.001

Gabriele, S., Chiaravalloti, F., & Procopio, A. (2017). Radar–rain-gauge rainfall estimation for hydrological applications in small catchments. *Advances in Geosciences*, *44*, 61–66. https://doi.org/10.5194/adgeo-44-61-2017

Gemini Data Loggers. (2017). Tinytag aquatic 2 data sheet. Retrieved November 22, 2017, from http://gemini2.assets.d3r.com/pdfs/original/2921-tg-4100.pdf

Golding, B. (2000). Quantitative precipitation forecasting in the UK. *Journal of Hydrology*, *239*(1–4), 286–305. https://doi.org/10.1016/S0022-1694(00)00354-1

Hannah, D. M., & Garner, G. (2015). River water temperature in the United Kingdom. *Progress in Physical Geography*, *39*(1), 68–92. https://doi.org/10.1177/0309133314550669

Hannah, D. M., Malcolm, I. A., & Bradley, C. (2009). Seasonal hyporheic temperature dynamics over riffle bedforms. *Hydrological Processes*, *23*(15), 2178–2194. https://doi.org/10.1002/hyp.7256

Hannah, D. M., Webb, B. W., & Nobilis, F. (2008). River and stream temperature: dynamics, processes, models and implications. *Hydrological Processes*, *22*(7), 899–901. https://doi.org/10.1002/hyp.6997

Harrison, D. L., Scovell, R. W., & Kitchen, M. (2009). High-resolution precipitation estimates for hydrological uses. *Proceedings of the Institution of Civil Engineers: Water Management*, *162*(2), 125–135. https://doi.org/10.1680/wama.2009.162.2.125

Herb, W. R., Janke, B., Mohseni, O., & Stefan, H. G. (2008). Thermal pollution of streams by runoff from paved surfaces. *Hydrological Processes*, *22*(7), 987–999. https://doi.org/10.1002/hyp.6986

Hester, E. T., & Bauman, K. S. (2013). Stream and retention pond thermal response to heated summer runoff from urban impervious Surfaces [1]. *JAWRA Journal of the American Water Resources Association*, *49*(2), 328–342. https://doi.org/10.1111/jawr.12019

Hofmeister, K. L., Cianfrani, C. M., & Hession, W. C. (2015). Complexities in the stream temperature regime of a small mixed-use watershed, Blacksburg, VA. *Ecological Engineering*, *78*, 101–111. https://doi.org/10.1016/J.ECOLENG.2014.05.019

Jacobson, C. R. (2011). Identification and quantification of the hydrological impacts of imperviousness in urban catchments: A review. *Journal of Environmental Management*, *92*(6), 1438–1448. https://doi.org/10.1016/j.jenvman.2011.01.018

Jones, M. P., Hunt, W. F., & Winston, R. J. (2012). Effect of urban catchment composition on runoff temperature. *Journal of Environmental Engineering*, *138*(12), 1231–1236. https://doi.org/10.1061/(ASCE)EE.1943-7870.0000577

Koch, J., & Stisen, S. (2017). Citizen science: A new perspective to advance spatial pattern evaluation in hydrology. *PLoS One*, *12*(5), e0178165. https://doi.org/10.1371/journal.pone.0178165

Laanaya, F., St-Hilaire, A., & Gloaguen, E. (2017). Water temperature modelling: Comparison between the generalised additive model, logistic, residuals regression and linear regression models. *Hydrological Sciences Journal*, 1–16. https://doi.org/10.1080/02626667.2016.1246799

Lange, J., & Haensler, A. (2012). Runoff generation following a prolonged dry period. *Journal of Hydrology*, *464–465*, 157–164. https://doi.org/10.1016/J.JHYDROL.2012.07.010

Met Office. (2003). Met Office Rain Radar Data from the NIMROD System. NCAS British Atmospheric Data Centre, 6th November 2018. http://catalogue.ceda.ac.uk/uuid/82adec1f896af6169112d09cc1174499

Met Office. (2018). Weather observations website. Retrieved June 15, 2018, from http://wow.metoffice.gov.uk/

Muller, C. L., Chapman, L., Grimmond, C. S. B., Young, D. T., & Cai, X. (2013). Sensors and the city: A review of urban meteorological networks. *International Journal of Climatology*, *33*(7), 1585–1600. https://doi.org/10.1002/joc.3678

Murase, H., Nagashima, H., Yonezaki, S., Matsukura, R., & Kitakado, T. (2009). Application of a generalised additive model (GAM) to reveal relationships between environmental factors and distributions of pelagic fish and krill: A case study in Sendai Bay, Japan. *ICES Journal of Marine Science*, *66*(6), 1417–1424. https://doi.org/10.1093/icesjms/fsp105

Nelson, K. C., & Palmer, M. A. (2007). Stream temperature surges under urbanization and climate change: Data, models, and responses. *Journal of the American Water Resources Association*, *43*(2), 440–452. https://doi.org/10.1111/j.1752-1688.2007.00034.x

NRFA. (2018). 28039—Rea at Calthorpe Park. Retrieved April 22, 2018, from https://nrfa.ceh.ac.uk/data/station/spatial/28039

Pedersen, L., Jensen, N. E., Christensen, L. E., & Madsen, H. (2010). Quantification of the spatial variability of rainfall based on a dense network of rain gauges. *Atmospheric Research*, *95*, 441–454. https://doi.org/10.1016/j.atmosres.2009.11.007

Rico-Ramirez, M. A., Liguori, S., & Schellart, A. N. A. (2015). Quantifying radar-rainfall uncertainties in urban drainage flow modelling. *Journal of Hydrology*, *528*, 17–28. https://doi.org/10.1016/J.JHYDROL.2015.05.057

Salvadore, E., Bronders, J., & Batelaan, O. (2015). Hydrological modelling of urbanised catchments: A review and future directions. *Journal of Hydrology*, *529*, 62–81. https://doi.org/10.1016/j.jhydrol.2015.06.028

Samuel, J., Coulibaly, P., & Metcalfe, R. A. (2011). Estimation of continuous streamflow in Ontario ungauged basins: Comparison of regionalization methods. *Journal of Hydrologic Engineering*, *16*(5), 447–459. https://doi.org/10.1061/(ASCE)HE.1943-5584.0000338

Sandoval, S., Torres, A., Duarte, M., & Velasco, A. (2014). Assessment of rainfall influence over water quality effluent of an urban catchment: A data driven approach. *Urban Water Journal*, *11*(2), 116–126. https://doi.org/10.1080/1573062X.2013.765492

Somers, K. A., Bernhardt, E. S., Grace, J. B., Hassett, B. A., Sudduth, E. B., Wang, S., & Urban, D. L. (2013). Streams in the urban heat island: Spatial and temporal variability in temperature. *Freshwater Science*, *32*(1), 309–326. https://doi.org/10.1899/12-046.1

Somers, K. A., Bernhardt, E. S., McGlynn, B. L., & Urban, D. L. (2016). Downstream Dissipation of storm flow heat pulses: A case study and its landscape-level implications. *JAWRA Journal of the American Water Resources Association*, *52*(2), 281–297. https://doi.org/10.1111/1752-1688.12382

Starkey, E., Parkin, G., Birkinshaw, S., Large, A., Quinn, P., & Gibson, C. (2017). Demonstrating the value of community-based ("citizen science") observations for catchment modelling and characterisation. *Journal of Hydrology*, *548*, 801–817. https://doi.org/10.1016/j.jhydrol.2017.03.019

Thorndahl, S., Einfalt, T., Willems, P., Nielsen, J. E., Ten Veldhuis, M.-C., Arnbjerg-Nielsen, K., … Molnar, P. (2017). Weather radar rainfall data in urban hydrology. *Hydrology and Earth System Sciences*, *21*, 1359–1380. https://doi.org/10.5194/hess-21-1359-2017

Tilburg, C. E., Jordan, L. M., Carlson, A. E., Zeeman, S. I., & Yund, P. O. (2015). The effects of precipitation, river discharge, land use and coastal circulation on water quality in coastal Maine. *Royal Society Open Science*, *2*(7), 140429. https://doi.org/10.1098/rsos.140429

Van Buren, M. A., Watt, W. E., Marsalek, J., & Anderson, B. C. (2000). Thermal enhancement of stormwater runoff by paved surfaces. *Water Research*, *34*(4), 1359–1371. https://doi.org/10.1016/S0043-1354(99)00244-4

Villarini, G., & Krajewski, W. F. (2010). Review of the different sources of uncertainty in single polarization radar-based estimates of rainfall. *Surveys in Geophysics*, *31*(1), 107–129. https://doi.org/10.1007/s10712-009-9079-x

Villarini, G., Mandapaka, P. V., Krajewski, W. F., & Moore, R. J. (2008). Rainfall and sampling uncertainties: A rain gauge perspective. *Journal of Geophysical Research*, *113*(D11), D11102. https://doi.org/10.1029/2007JD009214

Walsh, C. J., Fletcher, T. D., & Burns, M. J. (2012). Urban stormwater runoff: A new class of environmental flow problem. *PLoS One*, *7*(9), e45814. https://doi.org/10.1371/journal.pone.0045814

Wilby, R. L., Johnson, M. F., & Toone, J. A. (2015). Thermal shockwaves in an upland river. *Weather*, *70*(3), 92–100. https://doi.org/10.1002/wea.2435

Wood, S. N. (2017). *Generalised additive models: An introduction with R*.

Wood, S. N. (2018). Package "mgcv." Retrieved from https://cran.r-project.org/web/packages/mgcv/mgcv.pdf

Zhang, F., Cai, X., & Thornes, J. E. (2014). Birmingham's air and surface urban heat islands associated with Lamb weather types and cloudless anticyclonic conditions. *Progress in Physical Geography*, *38*(4), 431–447. https://doi.org/10.1177/0309133314538725

How to cite this article: Croghan D, Van Loon AF, Sadler JP, Bradley C, Hannah DM. Prediction of river temperature surges is dependent on precipitation method. *Hydrological Processes*. 2019;33:144–159. https://doi.org/10.1002/hyp.13317